

Annual Report, 2000
Crustal Deformation Processes, Seismicity, and the Gutenberg-Richter Distribution
Steven G. Wesnousky
University of Nevada, Reno

Our research progressed on two fronts, each aimed at understanding the relationship of earthquake frequency statistics to mappable characteristics of active faults. The first continues our exploration of the relationship between fault length and fault slip rate. Our data set has grown to include 258 faults for which geologically determined Holocene and Late Pleistocene slip rates have been reported. The compilation now includes faults from Japan, California, the Basin and Range, New Zealand, China, and selected sites from around the globe.

When fault slip rate is plotted against fault length (Fig. 1), two gross relationships emerge. Fault slip rate scales positively with fault length for strike-slip systems (Fig. 2a). This positive correlation may reflect the following: (1) Slip vectors in strike-slip systems are aligned with fault growth direction; and (2) Displacements in strike-slip zones tend to organize along discrete throughgoing zones as strike-slip offset accumulates across the zone of shear. Therefore, as strike-slip faults accumulate slip and lengthen, to first order their slip rates may also tend to increase.

In contrast to strike-slip systems, no correlation between fault length and fault slip rate is observed in dip-slip systems (Figs. 2b, 2c). The lack of correlation between length and slip rate in dip-slip systems occurs across all tectonic regions analyzed, and for both normal (Fig. 2b) and reverse (Fig. 2c) faults.

The lack of correlation of slip rate with fault length in normal fault systems may reflect: (1) Slip vectors are perpendicular to fault growth direction, so that accumulated slip and the slip rate are not necessarily linked to fault length; (2) Deviations from displacement/length scaling occur during normal fault linkage such that slip rate variation may be independent of fault length. Limitations in our data set may also obscure a relationship between normal fault length and fault slip rate: the longest normal faults in our data set are limited in length by gravitational and restoring forces, and the longest normal faults are nearly an order of magnitude shorter than the longest strike-slip faults. Also, longer recurrence intervals (or lower slip rates) introduce more uncertainty to slip rate estimates. The lack of correlation of slip rate with fault length in reverse fault systems may reflect many of the same considerations.

Future effort on this front will be aimed toward (1) further understanding the mechanics of crustal deformation responsible for the difference observed between dip-slip systems and strike-slip systems, (2) understanding slip rate/fault length relationships for normal faults in the context of complex normal fault growth and linkage, and (3) further subdividing our analysis by tectonic region and more closely examining local fault geometries for possible interactions.

Our second area of concentration addresses the nature of the Gutenberg-Richter distribution. Regional earthquake statistics are known to satisfy the Gutenberg-Richter distribution, but the question of whether seismicity of individual faults satisfies the relation remains a source of discussion. We continue to take an empirical approach to this problem by examining magnitude-frequency distributions for increasingly larger crustal volumes around major faults. In this manner, we aim to determine the physical

processes responsible for the observed Gutenberg-Richter statistics over broad regions, and whether those processes can be attributed to slip on the fault in question. The approach is illustrated below.

An active fault map for California and Nevada is shown in **Figure 3**. Boxes of 20 km width and increasingly greater length are placed over both the northern and southern San Andreas Fault. The smallest boxes are centered near the middle of the 1906 and 1857 earthquake ruptures, and increasingly longer boxes extend bilaterally from those points. Using a similar approach, we also examine the consequence of increasing the width as well as the length of the boxes, with each increasingly larger box sampling a greater volume of off-fault crust. The seismicity from a subset of these boxes is presented in **Figures 4a** through **4d** as a set of cumulative magnitude-frequency curves normalized to the number of events per year. In addition to the instrumentally recorded seismicity, we have also included from paleoseismic studies an estimate of the frequency of the largest slip events in each box. For example, it is reported by Sieh (1984) and Sieh, et al (1989), that a slip of at least 0.5m occurs on average each 132 years along the southern section of the San Andreas fault. This amount of slip corresponds to a release of seismic moment in the 20 x 20 km box equal to $M_0 = (3.3 \times 10^{11} \text{ dyne/cm}^2) (15 \text{ km fault width}) (20 \text{ km box length}) (0.5 \text{ m of displacement}) = 4.5 \times 10^{25} \text{ dyne-cm}$, which is equivalent to a $M_w=6.4$ event in the 20 x 20 km box (and accordingly greater for longer boxes) each 132 years. Thus, the magnitude of the largest events for each box represented in **Figures 4a** through **4d** reflects only the amount of moment released within the associated box and not that released on the entire fault. In this manner, we can place a firm minimum limit on the cumulative number of the largest expected earthquakes in each box and ask whether or not extrapolation of the instrumentally recorded statistics predict the frequency of occurrence of the largest slip events for the associated crustal volume. Results from our analysis of the southern San Andreas Fault were included in the 1999 Annual Report and are summarized here.

For each of the boxes that extends along the length of the southern San Andreas Fault, extrapolation of the curves from lesser to greater magnitudes underestimates the frequency of occurrence of largest expected slip events in the boxes (**Figure 4a**). Earthquake frequency statistics along the fault thus appear to be better described by the characteristic earthquake model than the Gutenberg-Richter distribution. When sampling wider as well as longer volumes of crust around the southern San Andreas, we observe that for small crustal volumes (20 x 20 km), the magnitude-frequency distribution displays a characteristic form (**Figure 4b**). When the box is increased in width as well as length to include the seismicity associated with the 1971 San Fernando and 1994 Northridge earthquakes, extrapolation of the statistics of instrumentally recorded events to predict the occurrence of larger events agrees with what has been observed geologically. In other words, along the southern San Andreas Fault, seismicity in the larger boxes shows a Gutenberg-Richter distribution.

We have since commenced similar analysis of the northern San Andreas Fault (**Figure 3**). The magnitude-frequency distributions that result from increasing the volume of the initial 20 x 20 km box along strike do not result in a Gutenberg-Richter magnitude-frequency distribution for box lengths less than 260 km (**Figure 4c**). The incorporation of the 1989 Loma Prieta earthquake sequence results in Gutenberg-Richter magnitude-frequency distributions of seismicity for volumes of crust with lengths greater

than or equal to 260 km (**Figure 4c**). The magnitude-frequency distributions resulting from an increase in box width as well as length also do not exhibit a Gutenberg-Richter form until seismicity associated with the 1989 Loma Prieta earthquake is incorporated. Magnitude-frequency distributions for seismicity within boxes longer and wider than 260 km show a Gutenberg-Richter form. The inclusion of the seismicity associated with the Hayward, Concord, and Rodgers Creek faults at smaller crustal volumes is not sufficient to result in a magnitude-frequency distribution with a Gutenberg-Richter shape (**Figure 4d**).

The shape of the magnitude-frequency distributions appears to progress from a characteristic to Gutenberg-Richter form only for crustal volumes of increasing width as well as length. This implies that, 1) the Gutenberg-Richter relation is only satisfied when seismicity from multiple sources is considered, or 2), the seismicity associated with an individual fault that satisfies the Gutenberg-Richter relation is not evenly distributed in time throughout the seismic cycle of the fault. Thus the observation that broad regions of seismicity satisfy the Gutenberg-Richter relation appears to be a consequence of combining the seismicity from multiple faults that are in various temporal positions within their respective seismic cycles. We are currently expanding our investigation to examine the effect of the temporal and spatial distribution of aftershocks on the relationship between magnitude and frequency. By looking at the effect of aftershocks, we can more accurately define the physical processes resulting in the observation that seismicity within broad regions satisfies the Gutenberg-Richter relationship.

Contact author for complete listing of references cited and used in fault data base.

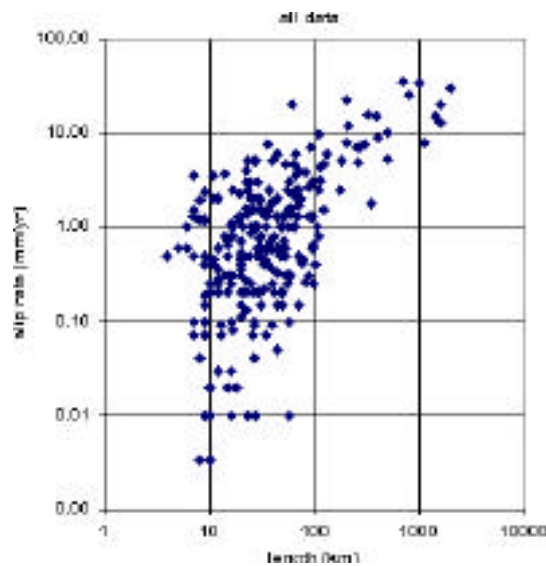


Figure 1. Fault slip rate versus fault length plotted for the entire data set.

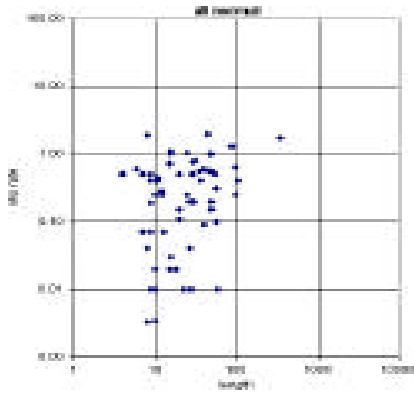


Figure 2a

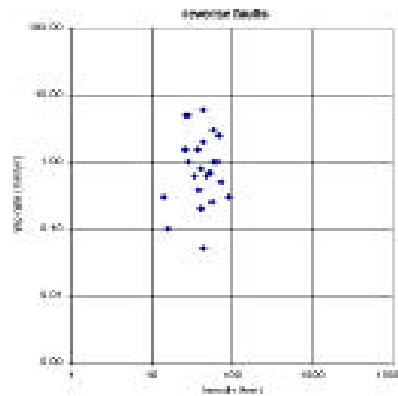


Figure 2b

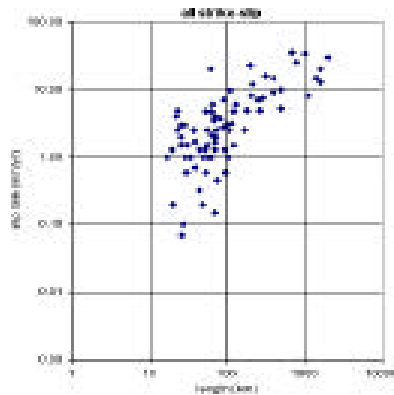


Figure 2c

Figures 2a, 2b, and 2c. Fault slip rate plotted against fault length for strike slip faults (2a), normal faults (2b), and reverse faults (2c).

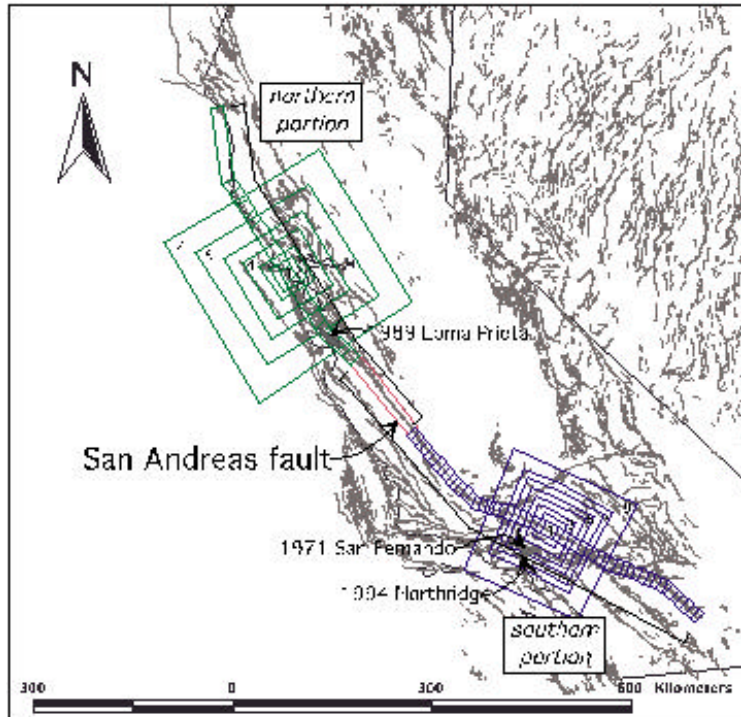
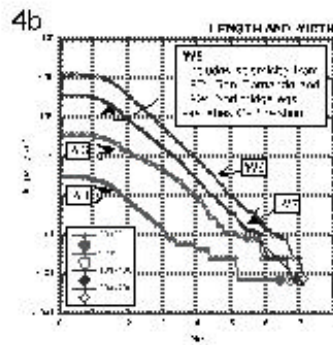
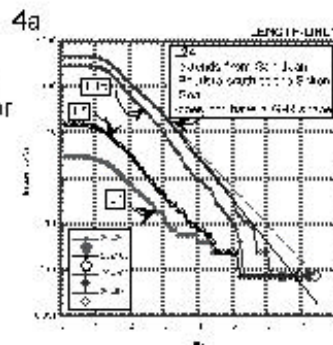


Figure 3. Active fault map of California and Nevada, including the northern and southern portions of the San Andreas fault. Magnitude-frequency distributions for seismicity within select boxes surrounding the fault are shown in Figure 4. Numbers within the boxes correspond to labels on the magnitude-frequency distributions. Approximate rupture zones for the 1971 San Fernando, the 1989 Loma Prieta, and the 1994 Northridge earthquakes are shown.

Figures 4a and 4b. Select magnitude-frequency distributions for seismicity within boxes along strike (4a), and along and perpendicular to strike (4b) of the southern portion of the San Andreas fault.



Figures 4c and 4d. Select magnitude-frequency distributions for seismicity within boxes along strike (4c), and along and perpendicular to strike (4d) of the northern portion of the San Andreas fault.

